Light-Controlled Actuation, Transduction, and Modulation of Magnetic Strength in Polymer Nanocomposites

*Johannes M. Haberl, Antoni Sánchez-Ferrer, Adriana M. Mihut, Hervé Dietsch, Ann M. Hirt, and Raffaele Mezzenga**

Remotely controlled actuation with wireless sensorial feed-back is desirable for smart materials to obtain fully computer-controlled actuators. A light-controllable polymeric material is presented, in which exposure to light couples with a change in magnetic properties, allowing light signal conversion into non-volatile magnetic memory. The same material can serve, additionally, both as actuator and transducer, and allows the monitoring of its two-way elastic shape-changes by magnetic read-out. In order to tune the macroscopic magnetic properties of the material, both the reorientation of i) shape anisotropic ferrimagnetic nano-spindles and ii) a mechanically and magnetically coupled liquid-crystalline elastomer (LCE) matrix are controlled. These materials are envisioned to have great potential for the development of innovative functional objects, for example, computer-controlled smart clothing, sensors, signal encoding, micro-valves, and robotic devices.

Controlling magnetic properties via external stimuli can open the way to new magneto-active materials.[1,2] Light can ideally activate magnetic response, since it is non-invasive and can be transferred wirelessly over large distances.[3] Nonetheless, due to the low magnetic susceptibility of organic matter, light-triggered magnetic changes in polymers remain difficult to be exploited. Here we present a polymeric material, in which exposure to light couples with a change in magnetic properties, allowing light signal conversion into non-volatile magnetic memory.

Photoresponsive magnetic materials span a broad spectrum of length scales, extending from a molecular scale with charge-transfer and spin-crossover,[2,4] to controlled domain wall motion in single crystals[5] and spin inversion with circular polarized light in bulk magnetic recording media.[6,7] However, the structural changes in all these materials are local and the macroscopic deformation is typically too small to serve in a broader context of applications. In contrast, polymeric elastomers allow high deformations but the occurrence of room-temperature ferromagnetism of polymers alone remains an exotic and weak effect.[8] In order to introduce a stronger, exploitable magnetic response, we proposed coupling the ferrimagnetic properties of embedded nanoparticles (NPs) having strong shape-anisotropy with the mechanical properties of the surrounding polymer matrix.[9,10] To introduce the photo-mechanical effect in organic systems, photo-isomerizing molecules have been incorporated as a switch to actuate liquid-crystalline (LC)[11] or crystalline organic materials.[12] However, due to the high absorption coefficient of incorporated NPs, such as, for instance, carbon nanotubes, a much more efficient actuation can be achieved by thermal relaxation effects after photo-excitation of the NPs in shape-memory polymer nanocomposites,[13] and liquid-crystalline elastomer (LCE) nanocomposites.[14] Nonetheless, these nanocomposites cannot offer any usable magnetic response due to the extremely low magnetic susceptibility of organic matter. Instead, we propose here to use anisotropic nanospindles from γ-Fe_2O_3 as nanofillers in LCEs, for which both magnetic and optical response[15] becomes pursuable. We then show that the oriented nanocomposite (OLCE) presented in this study, exhibits a unique two-way reversible actuation as a function of two different external stimuli, either illumination or temperature change, with a simultaneous change of ferrimagnetism and we demonstrate that remote controlled actuation can be monitored by magnetic means. The new material is proposed as the missing extension to the information storage materials discussed above, to gain access to applications ranging from signal manipulation to artificial muscles in computer-controlled robotic devices.

The LCEs with covalently incorporated magnetic NPs were obtained from surface functionalized core-shell maghemite nanospindles. These NPs were embedded into a hydroxyl-terminated LC polyester and mutually crosslinked with a triisocyanate, as previously reported.[9] A macroscopically oriented OLCE nanocomposite was obtained from a similar mixture using a two-step crosslinking procedure.[16] This has required an intermediate deformation step to orient the LC and to

J. M. Haberl, Dr. A. Sánchez-Ferrer, Prof. R. Mezzenga
ETH Zürich, Department of Health
Science and Technology
8092, Zürich, Switzerland
E-mail: raffaele.mezzenga@hest.ethz.ch
Dr. A. M. Mihut,[+] Dr. H. Dietsch[++]
Adolphe Merkle Institute & Fribourg Center for Nanomaterials
University Fribourg
1723, Marly, Switzerland
Prof. A. M. Hirt
ETH Zürich, Department of Earth Science
8092, Zürich, Switzerland
[+]Present address: Physical Chemistry, Department of Chemistry, Lund University, 22100 Lund, Sweden
[++]Present address: BASF SE, Formulation Platform, 67056 Ludwigshafen am Rhein, Germany

DOI: 10.1002/adfm.201304218

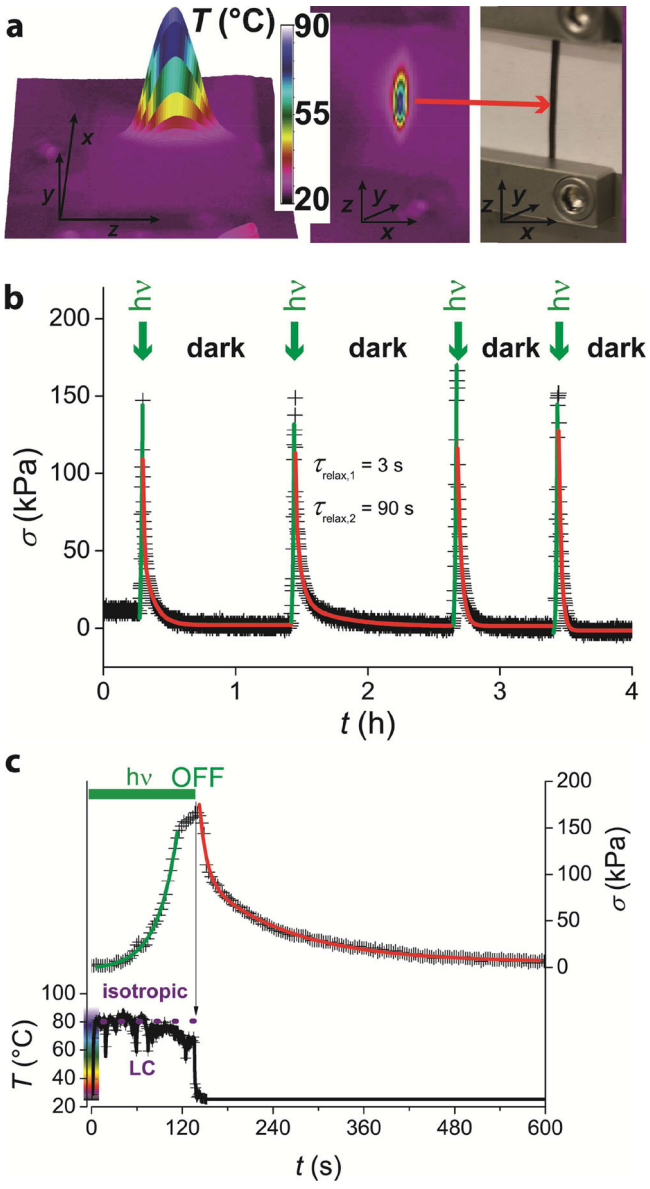

Figure 1. Laser-light induced heating and stress of the LCE nanocomposite. a) False-color infrared emission peak at position of laser-line target on the sample with the corresponding color map. b,c) Laser-light stimulated polymer-relaxation stress-cycles of OLCE measured at room-temperature (green and red curves are the corresponding excitation and relaxation fits, respectively) correlated to the light-induced temperature effect (c).

induce a prolate shape of the Gaussian polymer chain conformation after the first crosslinking step, which was fixed in the curing process.

In order to test the effect of light absorption on these nanocomposites, mechanical experiments were combined with monochromatic irradiation. The temperature effect was visualized by a thermo-camera as shown in **Figure 1**. Due to the high absorption coefficient of maghemite at 532 nm,[15] and its predominant thermal relaxation after the excitation, green light irradiation can be used to heat the LCE matrix beyond its LC phase transition (smectic-isotropic) temperature. When fixed from both extremes in a tensile stage, the OLCE nanocomposite operates as a light sensor and generates a maximum isostatic stress of $\sigma = 160$ kPa from a laser-line generator with an illuminated volume of 2.5 mm^3 and an excitation time of 140 s. When the light is turned off, the sample relaxes with two time constants: $\tau_{relax,1} = 3$ s associated to the polymer relaxation in the isotropic phase and $\tau_{relax,2} = 90$ s associated to the polymer recovery of the LC phase. Thus, the light-induced temperature change is responsible for the polymer conformation change, similar to the effect induced by temperature changes in presence of an external temperature source. A photo-energy actuator is alternatively obtained when the sample is kept free from one extreme restriction. This is evaluated in detail in a second stage: Thermoelastic experiments were performed in order to analyze the performance of the reversible shape change of the OLCE nanocomposite (**Figure 2**a). The polymer chains are relaxed into the spherical Gaussian chain distribution by heating to 100 °C in the isotropic phase ($\lambda = 1.0$). During cooling below the clearing temperature T_c, the aspect ratio of the sample changes and the sample reaches the length $\lambda = 1.15$, when the oriented LC phase is recovered and aligned according to the network restriction that was imprinted during the synthesis. Simultaneously, the polymer chain distribution becomes prolate. Upon heating, the enthalpy restriction of the LC phase is removed and the polymer relaxes back into its initial spherical Gaussian chain distribution.[16,17] It is interesting to note that in the present OLCE nanocomposite, there is a strong hysteresis between the heating and the cooling curve (Figure S1, Supporting Information). Similar hysteresis behavior is untypical for LCEs, but it is commonly associated with semi-crystalline phase changes in two-way actuators.[18] Due to the absence of crystalline peaks in the X-ray patterns, the behavior of this material is attributed to the kinetic effects of the triethylene oxide chain-segments.

To evaluate the nanostructural change during these temperature cycles quantitatively, a reorientation model is applied (Figure 2b). Based on the theory for ideal elastomers and a Poisson ratio of 0.5, all objects in the material are assumed to reorient due to simple geometric constraints.[19] Their orientation vector change upon deformation λ, which is identical to the transformation of any position vector θ_0 to θ, following:

$$\theta = \arctan\left(1/\sqrt{\lambda^3}\tan\theta_0\right) \quad (1)$$

Thus, the orientation distribution of the NPs, $dP/d\theta$, can be calculated from:

$$\frac{dP}{d\theta} = \frac{dP}{d\theta_0}\cdot\frac{d\theta_0}{d\theta} = \frac{dP}{d\theta_0}\cdot\left(\frac{d\arctan\left(\sqrt{\lambda^3}\tan\theta\right)}{d\theta}\right)$$
$$= \frac{dP}{d\theta_0}\cdot\left(\lambda^{3/2}\sin^2\theta + \lambda^{-3/2}\cos^2\theta\right)^{-1} \quad (2)$$

where $dP/d\theta_0$ is used as normalization constant of initially non-oriented objects.

Using this approach azimuthal scattering curves can be fitted with one parameter δ that is used instead of λ, with an expected value of $\delta/\lambda = 1$ for ideal elastomers. The evaluation

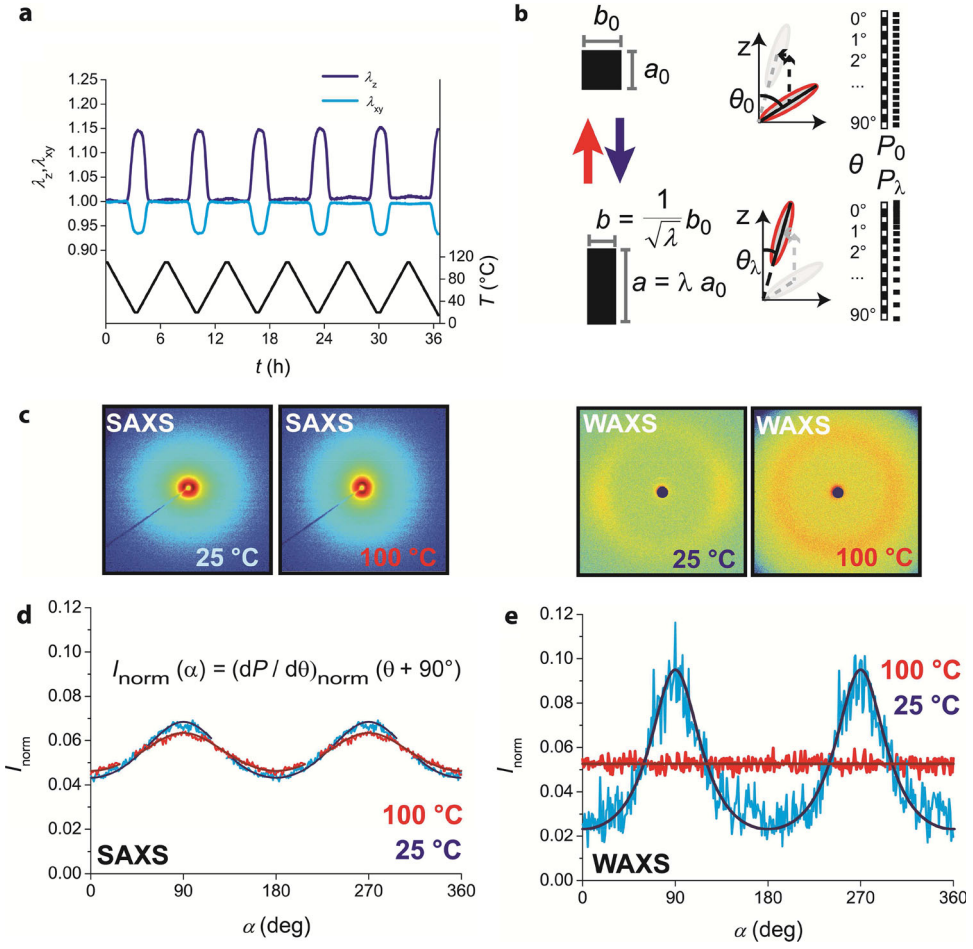

Figure 2. Actuation and structure analysis of the OLCE nanocomposite. a) Thermoelastic length changes in temperature cycles of the OLCE nanocomposite. b) Objects orientation vectors (P) in an ideal elastic material (constant volume) obeying the applied deformation $\lambda = a/a_0$ by reorientation from θ_0 to $\theta\lambda$. c) 2D X-ray scattering patterns at 25 and 100 °C in the small-angle (SAXS) and wide-angle (WAXS) region. d) The azimuthal scattering intensity in the SAXS region, and the corresponding fitting curve $I(\alpha) = (\delta^{3/2}\cos^2\alpha + \delta^{-3/2}\sin^2\alpha)^{-1}$, where $\delta = 1.16$ at 25 °C and $\delta = 1.10$ at 100 °C, and e) in the WAXS region, where $\delta = 1.6$ at 25 °C and $\delta = 1.0$ at 100 °C. In both cases α is taken as $\theta + 90°$.

further assumes scattering objects with infinite aspect ratio, as in Hermans' order parameter calculation,[20,21] so the population curve is shifted 90° to the scattering curve.

Based on this model, the orientational behavior of the LCE and the LCE nanocomposites were tested in mechanical and X-ray scattering experiments. The corresponding stress-strain curves are shown in Figure S2 (Supporting Information). In the LCE nanocomposites an increased modulus is obtained with higher particle contents and the network is strengthened in comparison to the neat reference sample LCE, as shown earlier.[10] In order to obtain the nanostructural changes, the azimuthal X-ray scattering distributions in the wide- and small-angle (WAXS, SAXS) were extracted as a function of applied deformation. In the WAXS region, the scattering peak at q = 14.4 nm^{-1} indicates the mesogen correlation length of the LC. The SAXS pattern at q = 0.153 nm^{-1} shows a correlation length associated to the core-shell ellipsoidal NPs.[9,10,22] High resolution scattering patterns for the mesogens were obtained from the reference sample LCE (**Figure 3**a,b) and from the nanocomposite LCE0.5 (Figure 3c, d) and for the NPs from the sample LCE10 (Figure 3e,f). The obtained scattering is shown with the fitting curves that were obtained from $I(\alpha) = (\delta^{3/2}\cos^2\alpha + \delta^{-3/2}\sin^2\alpha)^{-1}$, where α is taken as $\theta + 90°$. The fitting parameter δ is presented in **Figure 4** as a function of the deformation λ. In comparison, the apparent order parameter $S_{apparent}$ is shown in Figure 4b, which is calculated from the fitting curves, similar to Hermans order parameter:[20,21]

$$S_{apparent} = \frac{1}{2}\frac{\int_0^{\pi/2}\frac{dP}{d\theta}(\theta)(3\cos^2-1)\sin\theta d\theta}{\int_0^{\pi/2}\frac{dP}{d\theta}(\theta)\sin\theta\, d\theta} \quad (3)$$

The definition of $S_{apparent}$, without background subtraction, is necessary for reproducibility reasons at the design limit for lim S ($\lambda \to 1$) = 0. Due to their direct relation, both parameters δ and $S_{apparent}$ can be discussed together, in comparison to the elastomer reorientation model, where $S_{apparent}$ is calculated for a theoretical curve with $\delta = \lambda$. Upon initial deformation, the LCs

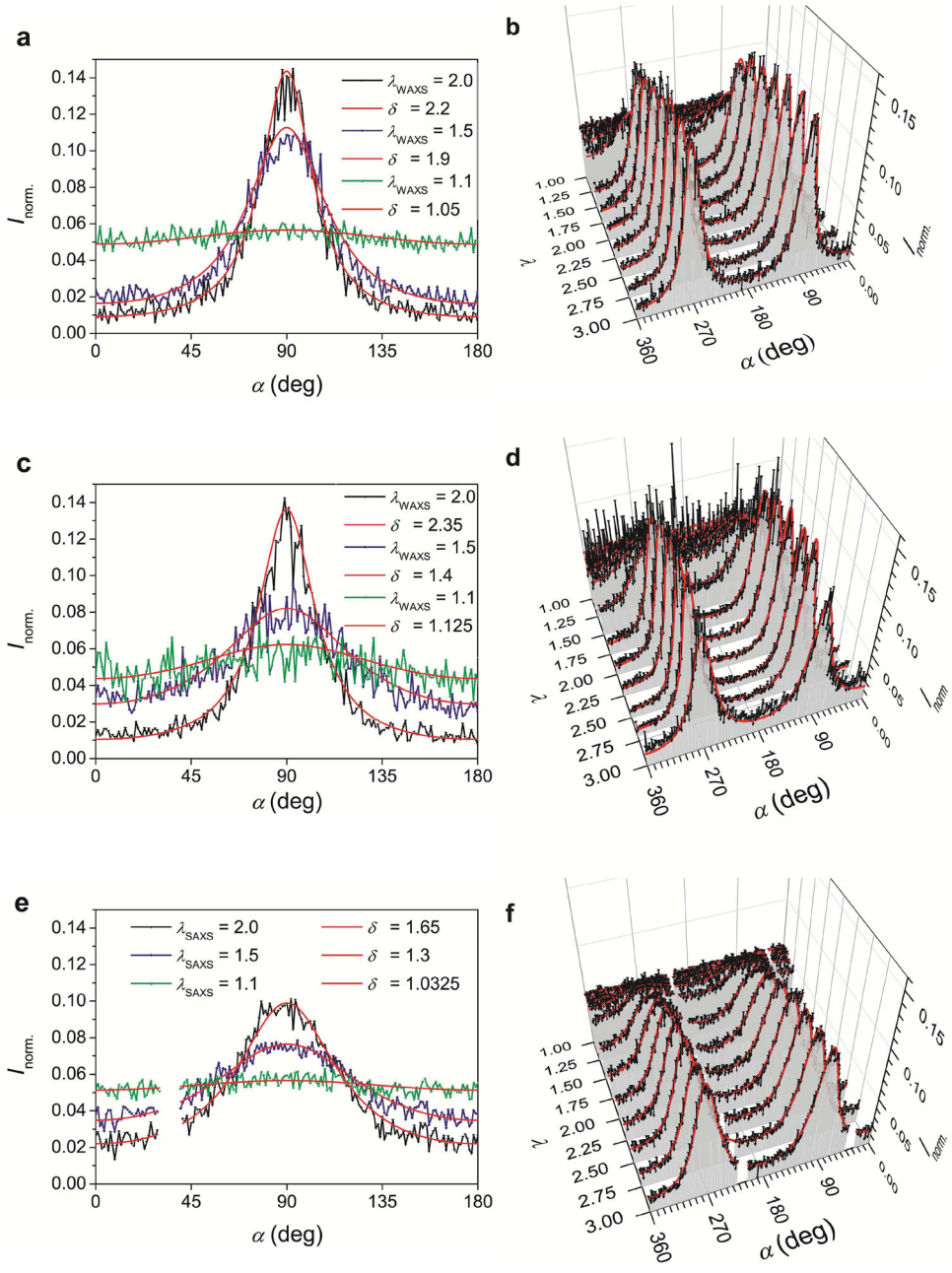

Figure 3. Azimuthal X-ray scattering distribution of a,b) the reference sample LCE and of c,d) the nanocomposite LCE0.5 at a scattering angle of q = 14.4 nm^{-1}, corresponding to the LC, and the azimuthal scattering intensity of the nanocomposite LCE10 (e,f) at q = 0.153 nm^{-1}, corresponding to the NPs. The fitting curves were obtained from $I(\alpha) = (\delta^{3/2}\cos^2\alpha + \delta^{-3/2}\sin^2\alpha)^{-1}$, where δ is used as fitting parameter, and λ is the applied deformation. α is taken as $\theta + 90°$. Note that for the NPs, the mean value of the two obtained peaks is taken to reduce noise and that data for the LC in the sample LCE10 and for the NPs in the sample LCE0.5 follow the same trend, but with significantly reduced signal-to-noise ratio and are not included here therefore.

in the reference sample LCE and in the nanocomposite LCE0.5 show an order parameter which is close to the predicted one from the reorientation model. At λ = 1.50 to 1.75, the order parameter of the mesogens increases beyond the prediction values, and grows slowly only from here on, falling back behind the prediction at high strain values. This is supported by earlier findings connected to the tensile modulus,[9,10] and similar studies on the order parameter of smectic LCEs.[23,24] At λ = 3, the experimental set-up induces defects due to slipping. For the NPs in LCE10, a different behavior is observed and the obtained order parameter stays constantly below the model value and the obtained values of the mesogens. This can be attributed to decoupling of the particles from the matrix and a missing LC alignment term in the free energy of the NP orientation below percolation. Please note that only due to our baseline treatment, the obtained apparent order parameters are below the conventionally obtained values for Hermans order parameter, which we used previously[9,10] and which can be taken in comparison.

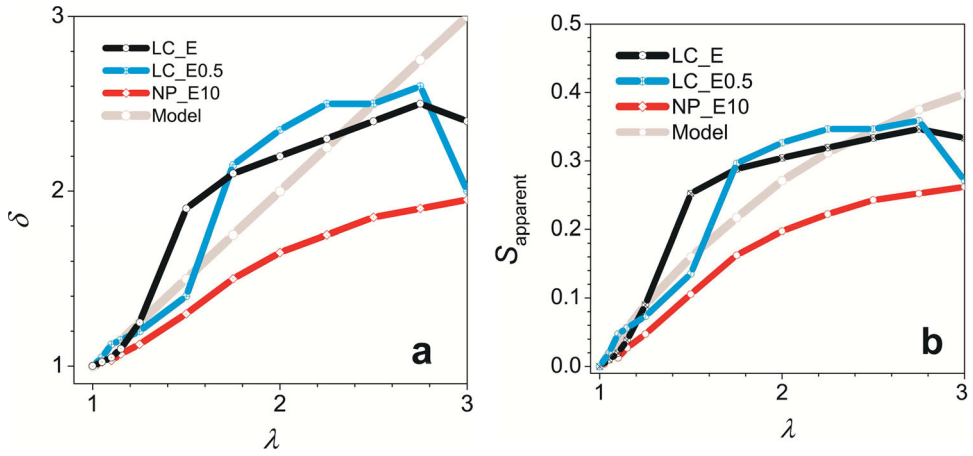

Figure 4. a) Fitting parameter δ and b) apparent order parameter $S_{apparent}$ as a function of the deformation λ for the LC in the reference sample LCE (black), the LC in the nanocomposite LCE0.5 (blue), and for the NPs in the nanocomposite LCE10.

In short, a continuous reorientation of the nanoparticles is noted during deformation.

Due to these results, also for the OLCE a continuous reorientation of the nanoparticles during the reversible deformation cycles is expected. This was verified by wide- and small-angle X-ray scattering (WAXS and SAXS) experiments, performed at 25 °C and 100 °C (Figure 2c). At high temperature and $\lambda = 1.0$, the isotropic scattering distribution in the WAXS region indicates the absence of order in the isotropic phase of the matrix (Figure 2d). The SAXS region, however, shows an anisotropic scattering, which is related to a remaining preferred orientation of the nanospindles due to the imprinted alignment during synthesis. After cooling to 25 °C into the LC phase, anisotropic scattering is observed in both the WAXS and SAXS regions. Quantitatively, upon cooling, the δ parameter increases from 1.10 to 1.16 in the SAXS region, and from $\delta = 1.0$ to $\delta = 1.6$ in the WAXS region. This is in agreement with the observations of higher orientation of the LC in comparison to the NPs in the non-oriented LCE stretching experiments and with the strong coupling of the LC and the elastic network in main-chain LCEs,[23,24] which is much more effective than the confinement that orients the NPs.[9,10]

The magnetic properties correlated to the change in orientation of the NPs were monitored as a function of temperature using a vibrating sample magnetometer (VSM). The experiments were carried out parallel and perpendicular to the imprinted axis of orientation (**Figure 5**). A strong magnetic field (H = 10 kOe) was first applied and then removed, thus imparting a remanent magnetization. This was then monitored during heating from room-temperature to the isotropic phase, and cooling back down to room-temperature. In the parallel configuration, upon heating through the phase transition temperature, the remanent magnetization decreases about 14%. The original magnetization is recovered to a large extend upon cooling. This is reflecting the reorientation of the NPs.[25,26] In perpendicular configuration, the change in remanent magnetization is weaker than in parallel configuration due to the two equivalent dimensions of expansion, x and y (Figure 2a) and the observed effects are dominated by thermal relaxation of remanence within the NPs, due to the adverse imposed magnetization direction in this experiment. Thus, upon heating, only a plateau of the remanent magnetization is reached during the expansion of the sample in the measuring direction due to the increasing population of particles oriented in this direction, as observed in the X-ray experiments. Upon cooling through the phase transition, the remanent magnetization recovers the original trend seen for the reference LCE nanocomposite, where no reorientation occurs.

In order to evaluate the equivalence of the temperature-induced and light-induced changes on the magnetic properties, temperature controlled and laser-light stimulated VSM measurements were compared (set-up is shown in **Figure 6**a). Experiments are shown for the polydomain non-reversibly actuating LCE nanocomposite reference samples in order to distinguish between the temperature effects and shape effects. The temperature dependent hysteresis curves are shown in Figure 6b. After stretching the polydomain sample to $\lambda = 2.0$, the LCE acquires a remanent magnetization of $M_{r\|} = 0.26$ emu g^{-1} in the hysteresis measurement. Then the polydomain was recovered upon heating the sample at 100 °C, and the hysteresis curves were measured at 100 and 25 °C showing a clear overlapping and the same value of $M_{r\|} = 0.16$ emu g^{-1} at $\lambda = 1$. This proves that there is no measurable change in the magnetic structure of the NPs within this temperature range. To correlate the magnetization change to the deformation, the remanent magnetization was measured upon a heating-cooling cycle. In Figure 6c, the obtained magnetization change is compared to the elongation λ_z obtained from a thermoelastic experiment on the LCE. At T_c, when the sample shortens, the magnetization decreases due to the randomization of the NPs main axis[9,10] and stays constant during cooling, as the NP orientation stays randomized. Additionally, the matrix is supporting the magnetic signal change in a constructive way, since calamitic biphenyl moieties have positive magnetic susceptibility anisotropy,[27] and the LC misaligns in the same manner as the NPs.[9,10]

The results of the hysteresis measurements before, after and during illumination (Figure 6d) are in perfect agreement with the temperature-induced changes shown above. These results importantly verify that upon the applied illumination the temperature inside of the particles is not high enough for

ADVANCED FUNCTIONAL MATERIALS
www.afm-journal.de

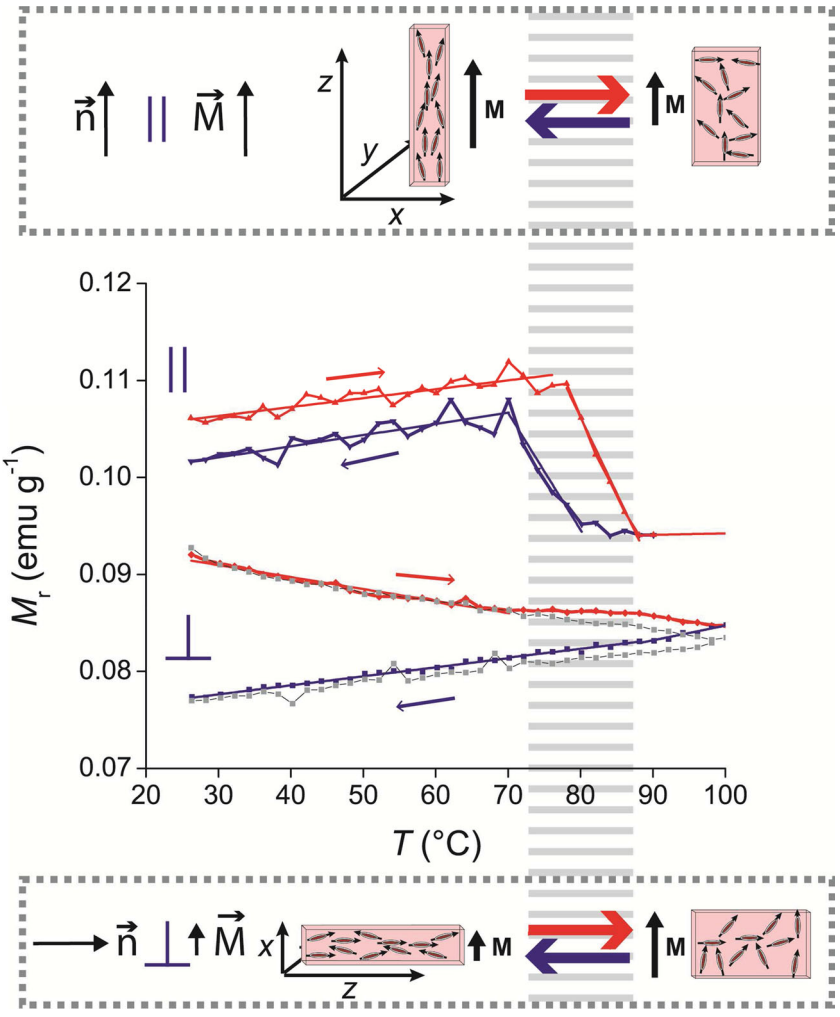

Figure 5. Reversible magnetization change of the OLCE nanocomposite. In a heating-cooling cycle after an initial magnetization (not shown) applied once parallel (∥) and once perpendicular (⊥) to the major susceptibility tensor of the sample, remanence is measured in the magnetization direction. In comparison, the non-oriented LCE nanocomposite is shown (grey symbols, shifted for overlap).

unblocking of the magnetization, and that magnetic properties are instead controlled by the orientation changes of the NPs driven by the organic LC matrix. In order to further evaluate the stability of the remanent magnetization and to demonstrate that this is exploitable, the relaxation behavior was measured first at $\lambda = 2.0$ at room-temperature, and then at $\lambda = 1.0$ at room-temperature and at 100 °C. The remanent magnetization value for the polydomain sample ($\lambda = 1.0$) was 45% smaller than for the stretched one ($\lambda = 2.0$). Upon illumination of the deformed sample, the relaxation of remanent magnetization switches from the relaxation curve at $\lambda = 2.0$ to the curve at $\lambda = 1.0$, in agreement with expectation based on sample deformation considerations (Figure 6e). In other terms, this change in remanent magnetization is strong enough to be comfortably measured and visible illumination can be converted into non-volatile magnetic memory.

In summary, we have presented a concept in which hybrid nanocomposites made of LCEs and core-shell maghemite nanospindles can be used on demand either as light-controlled actuators, transducers or magnetic storage devices. Light actuates these nanocomposites based on photothermal effects rising the materials internal temperature above the LC transition of the organic matrix without distortion of the inorganic structure. Thus, both light and temperature can be used to trigger the LCE nanocomposites and make them performing the desired function. These materials are perfect candidates for the targeted construction of fully computer-controlled actuators and sensors.

Experimental Section

The LCE nanocomposites were synthesized similarly to previously described procedures for the synthesis of LCE nanocomposites[10] and single-domain LCEs.[16] To obtain the orientation, a two-step crosslinking was performed following Küpfer et al.[16] After an initial crosslinking step in DCM-atmosphere during 1 h at room temperature, the slightly crosslinked LCE nanocomposite gel was cut into stripes and these were stretched to approximately twice of the original length and fixed in this position. The solvent was allowed to evaporate and the stretched LCE nanocomposite was heated to 80 °C for 48 h. The soluble content in the final OLCE nanocomposite was removed by extracting with $CHCl_3$ and acetone three times. The OLCE nanocomposite had a solid content of 90%, a volumetric swelling parameter (volume of $CHCl_3$-swollen elastomer to dry elastomer) of $q = 7.4$, and a volumetric swelling anisotropy of $\Sigma = 1.1$, where $\Sigma = \alpha_\perp/\alpha_\parallel - 1$ and the swelling ratio α_i is the ratio of $CHCl_3$-swollen length to dry length of the LCE in each direction. The reference sample LCE without orientation had a solid content of 86%, a swelling parameter of $q = 8.8$, and a swelling anisotropy of $\Sigma = 0$. Thermoelastic experiments were performed using a Julabo FE32-HN refrigerated-heating circulator. Equilibrated heating was performed in steps of 2 K with 30 min equilibration time for each step. In order to simulate fast processes during light-stimulated heating, experiments were done at 1 K min^{-1}. High resolution pictures were taken every 2 min with a computer controlled Canon EOS 550 digital camera equipped with a Canon macro lens EF 100 /2.8 L. In order to avoid bending of the elastomer, the sample was permanently equipped with a constant weight equivalent to about 0.03 MPa stress, depending on the shape of the sample. Small-angle and wide-angle X-ray scattering (SAXS and WAXS) experiments were performed using a Rigaku MicroMax-002+ microfocused beam (40 W, 45 kV, 0.88 mA) with the $\lambda_{Cu\ K\alpha} = 0.15418$ nm radiation in order to obtain direct information on the scattering patterns. The scattering intensities were collected by a Fujifilm BAS-MS 2025 imaging plate system (15.2 cm × 15.2 cm, 50 μm resolution) and a 2D Triton-200 X-ray detector (20 cm diameter). An effective scattering vector range of 0.05 nm^{-1} < q < 25 nm^{-1} was obtained, where q is the scattering wave vector defined as $q = 4\pi \sin\theta / \lambda_{Cu\ K\alpha}$ with a scattering angle of 2θ. For the order parameter of the NPs, the SAXS patterns were evaluated at low scattering angles ($q = 0.15$ to 1.0 nm^{-1}) and were related to the NPs orientation following an integration intensity procedure as previously reported.[9,10,22] The scattering is weak in a neat LCE reference sample at this scattering angle.[9] For stress-free relaxation conditions, high and

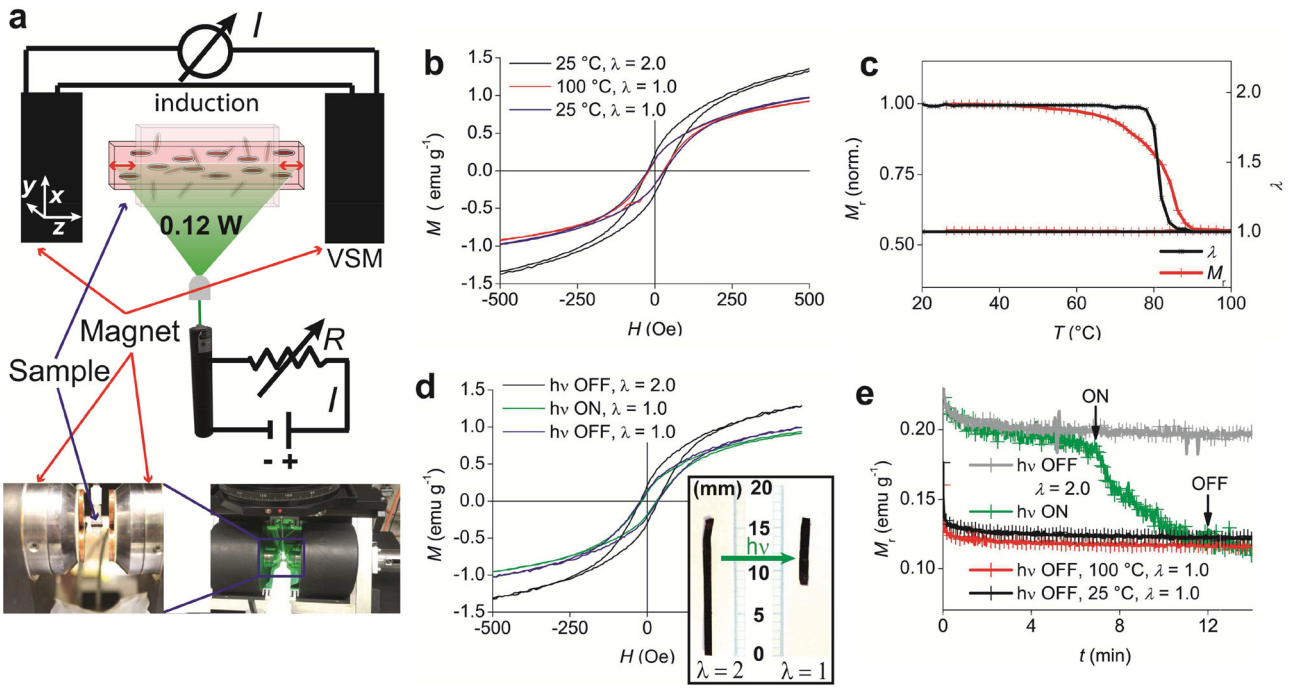

Figure 6. Magnetization behavior of the shape-memory LCE nanocomposite upon temperature change and light stimuli. a) Experimental set-up with laser-light source and vibrating sample magnetometer (VSM) measurement. b) Magnetic hysteresis of the deformed LCE nanocomposite at $\lambda = 2.0$ and $\lambda = 1.0$ at room-temperature, and at $\lambda = 1.0$ at 100 °C. c) Comparison of M_r and λ, which indicates the simultaneous transition of magnetic properties and sample-shape upon heating. d) Magnetic hysteresis of the deformed LCE nanocomposite at $\lambda = 2.0$ and $\lambda = 1.0$ without light stimulus, and at $\lambda = 1.0$ measured during light illumination. The inset shows the sample before and after light illumination. e) The relaxation behavior of the remanent magnetization M_r at $\lambda = 2.0$, $\lambda = 1.0$ at room temperature, at $\lambda = 1.0$ at 100 °C, and upon illumination at room temperature.

low-temperature measurements were performed on different sample holders, thus the *z*-axes are shifted 90° one to another in the obtained patterns. In order to reduce the noise level for the evaluation, an average of the two corresponding azimuthal peaks is taken with respect to the C_2 symmetry and shown in Figure 2d and Figure 2e. For the scattering data of a sample in the SAXS and respectively WAXS, a constant weak scattering background was determined by fitting at all strain regions and it was subtracted from the azimuthal intensities to compensate random scattering. Tensile test measurements and light stimulated relaxation-force measurements were performed on a Linkam TST350 thermostated tensile stress testing (TST) system, computer controlled by a T95 LinkSys apparatus. As a laser-light source, a commercial 200 mW Nd:YAG laser with frequency doubling to 532 nm was equipped with a Lytron NG 2500 constant power supply and a voltage of 3 V was applied allowing a current of 500 mA. The LCE reference sample without NPs is not responding to such stimulus. A laser line generator with an opening angle of 30° was used to control the sample illumination. The laser-light power output on the sample was measured with a XR2100 optical power meter from X-Cite at 532 nm, equipped with a XP 750 objective plane power sensor with an uncertainty of ± 5%. For the evaluation of the reorientation, measurements were performed at 60 °C with a deformation speed of 10 μm s^{-1} and 30 min equilibration time. The infrared light images were taken with a TIM 160 thermo imager from Micro-Epsilon. It was equipped with a 25° x 17° lens collecting a spectral range of 7.5 to 13 μm with a system accuracy of ± 2° and a temperature resolution of 0.08 K. Magnetic hysteresis and magnetization values were measured on a PMC MicroMag 3900 vibrating sample magnetometer (VSM) in fields from $H = -10$ kOe to 10 kOe at 25 °C, using the LCE composite after stretching to a deformation of $\lambda = 2.0$ and the OLCE composite as synthesized. Temperature was controlled with the inbuilt oven that had to be removed from the magnet for the laser illumination. All $\lambda = 1.0$ measurements were collected after the first stimulus application (heating or/and light) and relaxation of the deformed sample; where necessary, that is, during a second illumination/heating step. It should be noted that for precise magnetic measurements the sample had to be confined to avoid bending of the elastomer, and thus the relaxation speed was limited due to surface friction.

Supporting Information

Supporting Information is available from the Wiley Online Library or from the author.

Acknowledgements

The authors gratefully acknowledge the help of I. Usov for calculations, J. Corsano, who built the mobile laser optics, H.-P. Hächler, who assisted in the magnetic measurements, the ETH EMEZ for providing their optical power meter, F. Iida for generously providing the IR camera, and the SNF NRP62 for financing the project.

Received: December 18, 2013
Published online: February 13, 2014

[1] T. A. Ostler, J. Barker, R. F. L. Evans, R. W. Chantrell, U. Atxitia, O. Chubykalo-Fesenko, S. El Moussaoui, L. Le Guyader, E. Mengotti, L. J. Heyderman, F. Nolting, A. Tsukamoto, A. Itoh, D. Afanasiev, B. A. Ivanov, A. M. Kalashnikova, K. Vahaplar, J. Mentink, A. Kirilyuk, Th. Rasing, *Nat. Commun.* **2006**, *3*, 666.
[2] S. Ohkoshi, K. Imoto, Y. Tsunobuchi, S. Takano, H. Tokoro, *Nat. Chem.* **2011**, *3*, 564–569.
[3] M. Moua, R. R. Kohlmeyer, J. Chen, *Angew. Chem. Int. Ed.* **2013**, *52*, 9234–9237.

[4] O. Satu, J. Tao, Y.-Z. Zhang, *Angew. Chem. Int. Ed.* **2007**, *46*, 2152–2187.
[5] E. Heintze, F. E. Hallak, C. Clauß, A. Rettori, M. G. Pini, F. Totti, M. Dressel, L. Bogani, *Nat. Mater.* **2013**, *12*, 202–206.
[6] C. E. Graves, A. H. Reid, T. Wang, B. Wu, S. de Jong, K. Vahaplar, I. Radu, D. P. Bernstein, M. Messerschmidt, L. Müller, R. Coffee, M. Bionta, S. W. Epp, R. Hartmann, N. Kimmel, G. Hauser, A. Hartmann, P. Holl, H. Gorke, J. H. Mentink, A. Tsukamoto, A. Fognini, J. J. Turner, W. F. Schlotter, D. Rolles, H. Soltau, L. Strüder, Y. Acremann, A. V. Kimel, A. Kirilyuk, Th. Rasing, J. Stöhr, A. O. Scherz, H. A. Dürr, *Nat. Mater.* **2013**, *12*, 293–298.
[7] C. D. Stanciu, F. Hansteen, A. V. Kimel, A. Kirilyuk, A. Tsukamoto, A. Itoh, T. Rasing, *Phys. Rev. Lett.* **2007**, *99*, 047601.
[8] Y. W. Ma, Y. H. Lu, J. B. Yi, Y. P. Feng, T. S. Herng, X. Liu, D. Q. Gao, D. S. Xue, J. M. Xue, J. Y. Ouyang, J. Ding, *Nat. Commun.* **2012**, *3*, 727.
[9] J. M. Haberl, A. Sánchez-Ferrer, A. M. Mihut, H. Dietsch, A. M. Hirt, R. Mezzenga, *Adv. Mater.* **2013**, *25*, 1787–1791.
[10] J. M. Haberl, A. Sánchez-Ferrer, A. M. Mihut, H. Dietsch, A. M. Hirt, R. Mezzenga, *Nanoscale*, **2013***5*, 5539–5548.
[11] M. Yamada, M. Kondo, J. Mamiya, Y. Yu, M. Kinoshita, C. J. Barrett, T. Ikeda, *Angew. Chem. Int. Ed.* **2008**, *47*, 4986–4988.
[12] O. S. Bushuyev, T. A. Singleton, C. J. Barrett, *Adv. Mater.* **2013**, *25*, 1796–1800.
[13] H. Koerner, G. Price, N. A. Pearce, M. Alexander, R. A. Vaia, *Nat. Mater.* **2004**, *3*, 115–120.
[14] Y. Ji, Y. Y. Huang, R. Rungsawang, E. M. Terentjev, *Adv. Mater.* **2010**, *22*, 3436–3440.
[15] J. Tang, M. Myers, K. A. Bosnick, L. E. Brus, *J. Phys. Chem. B* **2003**, *107*, 7501–7506.
[16] J. Küpfer, H. Finkelmann, *Macromol. Chem., Rapid Commun.* **1991***12*, 717–726.
[17] M. Warner, E. M. Terentjev, Liquid Crystal Elastomers, Oxford University Press, Oxford, **2007**.
[18] T. Chung, A. Romo-Uribe, P. T. Mather, *Macromolecules* **2008**, *41*, 184–192.
[19] S. V. Ahir, A. M. Squires, A. R. Tajbakhsh, E. M. Terentjev, *Phys. Rev. B* **2006**, *73*, 0854201–0854212.
[20] G. R. Mitchell, A. H. Windle, Orientation in liquid crystal polymers, Publ. D. C. Basset, Elsevier Applied Science, London, New York **1988**, ch. 3, pp.115.
[21] J. J. Hermans, P. H. Hermans, D. Vermaas, A. Weidinger, *Recueil des Travaux Chimique des Pays-Bas* **1945**, *65*, 6, 427–447.
[22] M. Reufer, H. Dietsch, U. Gasser, A. Hirt, A. Menzel, P. Schurtenberger, *J. Phys. Chem. B* **2010**, *114*, 4763–4769.
[23] A. Sánchez-Ferrer, H. Finkelmann, *Macromolecules* **2008**, *41*, 970–980.
[24] A. Sánchez-Ferrer, H. Finkelmann, *Macromol. Rapid Commun.* **2011**, *32*, 309–315.
[25] E. C. Stoner, E. P. Wohlfarth, *Philos. Trans. R. Soc. A*, **1948**, *240*, 599–624.
[26] R. C. O'Handley, Modern Magnetic Materials, Wiley-Interscience, New York, USA **2000**.
[27] A. Buka, W. H. de Jeu, *J. Physique* **1982**, *43*, 361–367.